Biophysical Chemistry 248 (2019) 16–27

Contents lists available at ScienceDirect

Biophysical Chemistry

journal homepage: www.elsevier.com/locate/biophyschem

Characterization of the self-assembly and size dependent structural properties of dietary mixed micelles by molecular dynamics simulations

Esra Tuncer, Beste Bayramoglu*

İzmir Institute of Technology, Food Engineering Department, Gulbahce Campus,Urla, Izmir 35430, Turkey

ARTICLE INFO

Keywords:
Dietary mixed micelles
Bile salts
Self-assembly
Cholate
POPC
Molecular dynamics simulations

ABSTRACT

The bile salts and phospholipids are secreted by the gallbladder to form dietary mixed micelles in which the solvation of poorly absorbed lipophilic drugs and nutraceuticals take place. A comprehensive understanding of the micellization and structure of the mixed micelles are crucial to design effective delivery systems for such substances. In this study, the evolution of the dietary mixed micelle formation under physiologically relevant concentrations and the dependence of structural properties on micelle size were investigated through coarse-grained molecular dynamics simulations. The MARTINI force field was used to model cholate and POPC as the representative bile salt and phospholipid, respectively. The micellization behavior was similar under both fasted and fed state concentrations. Total lipids concentration and the micelle size did not affect the internal structure of the micelles. All the micelles were slightly ellipsoidal in shape independent of their size. The extent of deviation from spherical geometry was found to depend on the micellar POPC/cholate ratio. We also found that the surface and core packing density of the micelles increased with micelle size. The former resulted in more perpendicular alignments of cholates with respect to the surface, while the latter resulted in an improved alignment of POPC tails with the radial direction and more uniform core density.

1. Introduction

Bile acids (BAs) and phospholipids (PLs) are natural surfactants, which have significant biological roles in the digestion of food and absorption of lipophilic nutraceuticals and drugs. They are secreted together with cholesterol from the gall bladder during digestion and form dietary mixed micelles in the duodenum. The role of dietary micelles is to enable the delivery of lipophilic molecules like dietary fats, drugs and nutraceuticals in the body, and thus, facilitate their molecular absorption from the small intestine to the bloodstream [1]. Therefore, a comprehensive understanding of the self-assembly process in the upper intestinal lumen and the structure of the dietary micelles is very important for an effective design of oral lipid-based delivery systems for poorly absorbed drugs and nutraceuticals.

Many biophysical studies have long been conducted in order to characterize the upper intestinal medium under fasted and fed states and to analyze the generic physical properties such as the morphology, size distribution and dynamics of dietary mixed micelles [2–13]. Despite the rigorous efforts made, there are still persisting gaps in the knowledge of mixed micelle formation and micelle structure due to the difficulties associated with the experimental methods. For example, it is impossible to determine the micellar structure at atomic level and also on the basis of individual aggregates owing to the highly mobile and dynamic (continuously dissociating and associating) nature of the micelles [14]. Fortunately, the advances in the computational power and techniques have enabled the researchers to attain a deeper understanding of these systems [15]. Being a deterministic method, molecular dynamics (MD) simulations are especially considered as a powerful tool to study the structure and dynamics of self-assembly systems reliably.

The first attempt to model human bile was the prominent study of Marrink and Mark [16]. They performed a number of atomistic MD simulations on model systems composed of 3α,7α,12α-trihydroxy-5β-cholanoate (cholate), 1-palmitoyl-2-oleoyl-sn-glycero-3-phosphocholine (POPC) and cholesterol, and analyzed the structures of the mixed micelles at atomic level. Due to the limited computational power of then, their simulations were restricted to a single micelle of predetermined size based on experimental estimates. Furthermore, in order to achieve the convergence of the systems at accessible time scales, they studied at the concentration of the human gall bladder, which is quite higher from duodenal concentrations. Ever since, MD simulations of bile salts (BSs) and PLs have been of great interest to other researchers owing to their importance in many different fields of applications. Some of the earlier attempts focused on the structure and aggregation

* Corresponding author.
E-mail addresses: esrakacar@iyte.edu.tr (E. Tuncer), bestebayramoglu@iyte.edu.tr (B. Bayramoglu).

https://doi.org/10.1016/j.bpc.2019.02.001
Received 1 October 2018; Received in revised form 27 January 2019; Accepted 1 February 2019
Available online 05 February 2019
0301-4622/

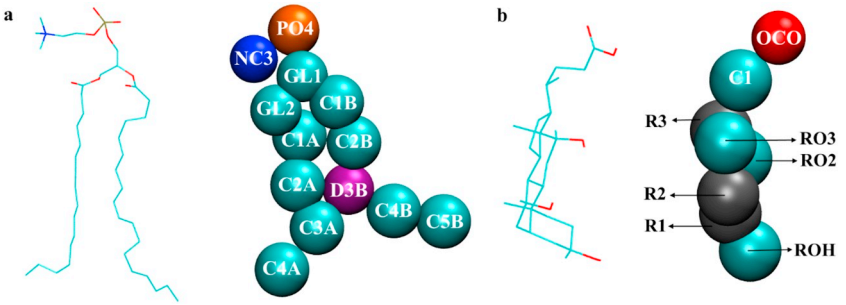

Fig. 1. Atomistic and coarse grained structures of (a) POPC and (b) CHOA (cholate). Hydrogen atoms are omitted in atomistic structures for visual clarity.

dynamics of simple dietary micelles (composed of BS molecules only) [17–20]. The subsequent atomistic-scale studies were directed towards both the simple and mixed micelles. Sayyed-Ahmad et al. [21] investigated the dependence of the structure of mixed micelles composed of cholate (CHOA) and dodecylphosphocholine (DPC) on concentration. Though, the concentrations and the ratios of PL-to-BS they used were still far beyond the duodenal conditions. Turner et al. [22] acquired important knowledge on the intermolecular interactions involved in the micelle formation through their MD simulations of glycocholate (GCHOA) and GCHOA-oleic acid (OA) mixtures. However, they restricted the self-assembly simulations to GCHOA micelles at the gall bladder concentration, and studied the incorporation of OAs into a single GCHOA micelle after its dilution to intestinal fed state concentration. Some researchers resorted to using coarse-grained force fields to probe larger length and time scales in order to gain a molecular-scale insight into the micellization process and the structural properties of simple and mixed micelles [23–27]. With the accumulation of knowledge and the advance of computational resources, recent studies have been targeted at investigating more sophisticated phenomena such as the effects of digestion products, cholesterol content, pH and inorganic salt content on the phase behavior of intestinal fluids [28–30].

The present work is the first of a series of manuscripts aiming at deepening the knowledge about the duodenal mixed micelles under different physiological conditions and the factors modulating the solvation of lipophilic molecules in them. The objectives of this contribution are two-fold. First, we aim to analyze and compare the dietary mixed micelle formation under two physiologically relevant duodenal concentrations; i.e., fasted and fed states. Secondly, a detailed characterization of the structural properties and their dependence on micelle size are aimed at. We believe it is important to expand our knowledge in this regard in order to have a better control on the use of dietary mixed micelles in different fields of applications. To the best of our knowledge, no such detailed structural analysis of the dietary mixed micelles as a function of the micelle size has been conducted before. The model bile lipids in our systems are cholate, which is accepted as the most representative structure of the BSs [31], and the zwitterionic POPC, which is a common PL in human bile. We chose to exclude cholesterol on the grounds of various studies showing that the concentration of cholesterol in the small intestine originating from the gall bladder is dilute [32,33], and thus its solubility in the dietary mixed micelles is very low [34,35]. Furthermore, it has been demonstrated that cholesterol does not have any significant effects on the micelle size, shape, structure or dynamics under dilute concentrations [27,30,36]. As MD simulations of self-assembly processes are rather demanding in terms of the length and time scales required to be probed for a satisfactory description of the phenomena, and atomistic simulations would computationally be too expensive to reach time scales up to several microseconds for such large systems, a coarser-level representation was adopted in this study. The MARTINI Force Field [37], which is a coarse-grained model originally developed for lipids was used in our simulations. The model has been improved over the past years to describe a wider range of biomolecular and polymeric systems [38–41]. Furthermore, its use in reproducing structures compatible with the atomistic simulations and experimental values has been shown before in several studies involving mixed micelles [26–28,42–44].

The rest of the paper is organized as follows. In the next section, the details of the system configurations in the self-assembly simulations and the simulation methodology are given. Then, the evolution of the mixed micelle formation under both fasted and fed states are analyzed, which is followed by a detailed size dependent characterization of the structural properties of the stable micelles. Finally, the results are discussed within the framework of previously proposed mixed micelle models in the literature. This manuscript will be followed by the outputs of an ongoing investigation on the effects of different types of fatty acids on the micellization and structure of mixed micelles, the complementary results of which are foreseen to be utilized in the design of drug or nutraceutical delivery systems (Tuncer and Bayramoglu, “in preparation”).

2. Methods

2.1. Details of the systems in self-assembly simulations

The concentrations of bile lipids (BSs + PLs) in the upper intestinal fluids differ depending on the state of digestion within the body. In order to model the fasted (before digestion) and fed state (during digestion) conditions, widely used BS:PL concentrations in various in vitro studies [45,46], 5:1.25 mM and 20:5 mM, respectively, were adopted in the construction of our systems. Note that the ratio of BS to PL concentrations is fixed to 4 in both states as this ratio is at which they are secreted in bile [46,47]. CHOA, which is the model BS in this work, is characterized by a hydrophilic and a hydrophobic face composed of 3 hydroxyl and 3 methyl groups, respectively. The model PL, POPC, is composed of a zwitterionic head group (composed of choline and phosphate moieties) attached to two hydrophobic fatty acid (oleoyl and palmitoyl) tails (Fig. 1). In the simulated conditions, cholate molecules are assumed to be in their negatively charged forms because of having a pKa value (~5.5), which is smaller than the intestinal pH (~7). The simulation media also contain Na^+ and Cl^- ions corresponding to a concentration of 150 mM NaCl to mimic the physiological conditions. Additional Na^+ ions were added to neutralize the systems. Sufficient amounts of water molecules were added to solvate each system to the desired concentration. As one of the objectives was to explore the effects of micelle size on structural properties, three systems of different sizes were studied at fasted state. The compositional details of each system can be found in Table 1. The simulation of a larger system at fasted state was prohibited due to overwhelming computational costs.

The coarse-grained (CG) MARTINI Force Field was used in the simulations. In MARTINI force field, generally 4 heavy atoms together with the associated hydrogens are represented by a single interaction site (bead). A higher resolution is used for ring structures, i.e., 2 to 3 heavy atoms and the associated hydrogens represent a single

Table 1
Number of molecules in the systems of self-assembly simulations at fasted and fed states. BS: bile salt, PL: phospholipid, CHOA: cholate.

	Fasted state (BS:PL = 5:1.25 mM)			Fed state (BS:PL = 20:5 mM)
System	A	B	C	D
Simulation box size	8000 nm^3	16,000 nm^3	20,000 nm^3	16,000 nm^3
CHOA	24	48	60	193
POPC	6	12	15	48
Na^+	746	1493	1867	1638
Cl^-	722	1445	1807	1445
Water	64,873	129,699	162,178	123,538

interaction site. The previously proposed models for POPC and CHOA molecules [27,48] were adopted in this study. POPC and CHOA are represented by 13 and 8 beads, respectively. There are two charged beads on the POPC head group representing the choline and the phosphate groups. Two beads of intermediate hydrophilicity are used to represent the glycerol ester moiety, and the remaining 9 beads are hydrophobic tail beads. CHOA is modeled by 6 beads (mapped on a 3:1 basis) forming the sterol body and 2 beads representing the short tail including the charged COO^- group. CG water molecules are comprised of four real water molecules and the CG beads of single atom ions are represented with their first hydration shell. The details of the CG structures together with their atomistic backbones are given in Fig. 1.

2.2. Simulation procedure and the analysis methods

MD simulations were performed using the GROMACS simulation package (version 5.1) [49] in cubic simulation boxes with periodic boundary conditions. The standard MARTINI force field parameters were used in the simulations. The non-bonded interactions were described by Lennard Jones 12–6 potential with a smooth shift to zero between 0.9 and 1.2 nm. For electrostatic interactions, a Coulombic potential with a relative permittivity of 15 and a shift function from 0 to 1.2 nm was used. Bond lengths of cholate molecules, if present, were constrained with Lincs algorithm. The initial velocities of the interaction sites were set according to the Maxwell-Boltzmann distribution corresponding to 310 K. The neighbor list was updated at every 10 steps. The Berendsen thermostat and barostat (with a time constant of 1 ps) were used [50] throughout the simulations for pressure and temperature couplings, respectively.

Initial configurations of single CG molecules of each type and the associated topologies were directly taken from MARTINI website (http://cgmartini.nl/index.php). The system configurations were initiated with placing all the CHOA and POPC molecules randomly in each simulation box. Then, the ions were added randomly, and the systems were solvated with CG water molecules. Firstly, energy minimization by the steepest descent method (step size of 0.01 nm) was applied to remove close contacts and to let the molecules forget their initial configurations. Then, pre-convergence runs of 10 ns (dt = 40 fs) in total at constant NPT (1 bar, 310 K) were conducted to relax the systems. In the meantime, whenever shrinkage in size occurred during pressure coupling, simulation boxes were resized and filled with additional CG water molecules to maintain the desired concentration of bile lipids. Once the system volumes (thus, the concentrations) were stabilized, the convergence runs were started at constant NPT with a time step of 20 fs. The convergence of simulations was monitored by the time evolution of the total energy, the number/weight-averaged aggregation numbers of the clusters and the number of free molecules within the system. The convergence simulations were followed by the production runs (using the same parameters), which lasted for 1 to 4 μs depending on the system. The sum of both the convergence and production runs for each system lasted for 5 μs in total.

For each system, the micelle that was observed for the longest time in the trajectory (belonging to the production runs) was chosen for detailed structural analyses. The time frames containing the selected micelle through the trajectory were used. The global structures were analyzed through the calculations of the radii of gyration (R_g), the ratios of the principle moments of inertia and the solvent accessible surface area (SASA). The local structures were examined through the radial density distributions (RDDs). The average angles between selected vectors in a molecule and with respect to the radial vector were calculated to further analyze the internal and surface orientations of the constituent molecules. All the analyses were performed by the relevant GROMACS tools over 150–300 ns of the trajectories belonging to production runs. The systems and the trajectories were visualized by VMD (version 1.9.2) [51].

3. Results and discussion

3.1. Evolution of the mixed micelle formation

The evolution of the micellization process in each system (Table 1) was examined separately. First, a cluster criterion was determined based on the inspection of the first minima of the RDFs between the individual CG beads of the CHOA and POPC molecules in a micelle. Accordingly, the molecules were considered to be in the same cluster if the distance between their closest beads was smaller than 0.6 nm. This cutoff value was also verified by analyzing the time dependent number of clusters with varying cutoff values (0.5 to 1.0 nm), and visual inspection of the snapshots of clusters. It was observed that the chosen cutoff resulted in the lowest noise level (data not shown). Moreover, the chosen cutoff is in agreement with similar studies conducted with different phospholipids using the MARTINI force field [42,52,53]. Using this cutoff value for the determination of clusters, the time dependent number of clusters and weight- (N_w) and number- (N_n) averaged aggregation numbers were calculated in order to trace the aggregation behavior of the systems. Calculations were performed as proposed by Sayyed-Ahmad and coworkers [21] using Eqs. (1) and (2), where A_n is the number of aggregates consisting of n molecules. The data were also used to check whether the simulations reached convergence.

$$N_n = \frac{\sum_{n>1} nA_n}{\sum_{n>1} A_n} \quad (1)$$

$$N_w = \frac{\sum_{n>1} n^2 A_n}{\sum_{n>1} nA_n} \quad (2)$$

The time evolution of the number of clusters, N_w and N_n are given in Fig. 2 for each 5th ns of the trajectory for the purpose of visual clarity. The number of clusters results were refined by excluding the clusters composed of two molecules. The expected trends of decreasing number of clusters and increasing N_w and N_n with time, which indicates the evolution towards convergence, are exemplified in all the systems. The correspondence of the time steps at which a sudden drop in the number of clusters and a sudden jump in N_w in each system is certainly not accidental. This indicates that the smaller aggregates that were self-assembled in the earlier stages of the simulations merge together to form larger aggregates in the course of the process, finally eventuating in stable micelles. The sharp peaks in N_w observed in Fig. 2b,c,d also correspond to the fusion moments of two aggregates into a single larger cluster. However, the structures formed were apparently unstable as they split into two soon. The simulation times after which no more consistent dramatic changes in the aggregation numbers and the number of clusters were observed were taken as the convergence points for the simulations, which correspond to roughly 1, 3, 4 and 1 μs for systems A, B, C and D, respectively. The increasing trend in the convergence times observed in the fasted state systems (towards system C)

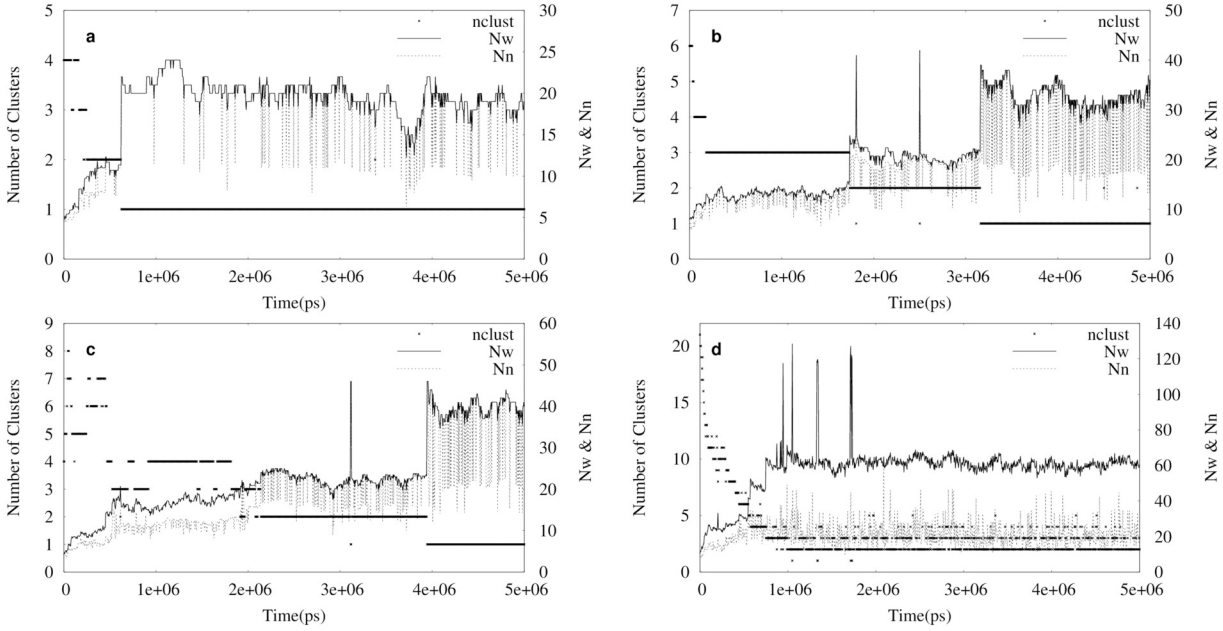

Fig. 2. The time evolution of the number of clusters (left y-axis) and weight- (N_w) and number- (N_n) averaged aggregation numbers (right y-axis) for systems A (Fasted-8000 nm^3), B (Fasted-16,000 nm^3), C (Fasted-20,000 nm^3) and D (Fed-16,000 nm^3). Results are given for each 5th ns of the trajectory (skipping the intermediate frames) for visual clarity. The number of clusters results were refined by excluding the clusters with two molecules.

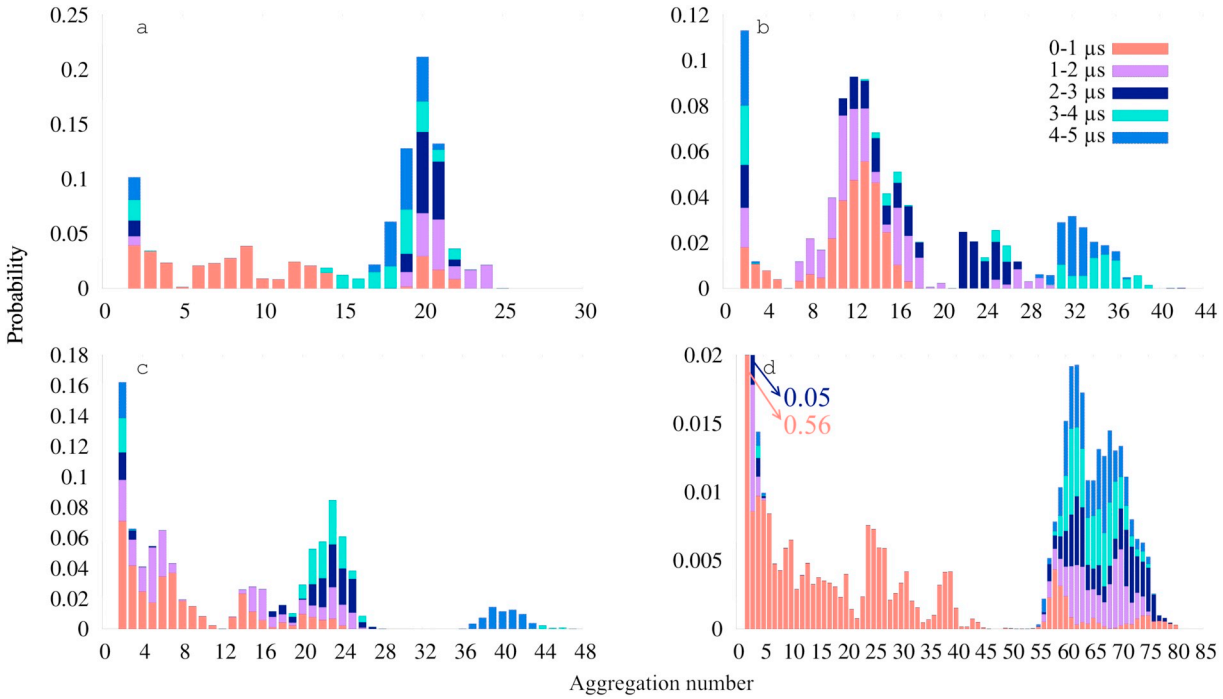

Fig. 3. The cumulative probability distributions of aggregation numbers as a function of time (block-averaged over 1 μs intervals) for systems A (Fasted-8000 nm^3), B (Fasted-16,000 nm^3), C (Fasted-20,000 nm^3), and D (Fed-16,000 nm^3). The regions including larger aggregation numbers in part (d) are omitted for clarity.

is the expected consequence of the significant increase in system sizes. A faster convergence was observed in the fed state system (D) compared to the fasted state system of similar size (system B), which is due to higher lipid concentrations in the former [22].

Although the mixed micelles obtained in each system were stabilized structures as implied by Fig. 2, the attainment of true thermodynamic equilibrium states in some of these systems did not seem applicable due to the limited system size and computation times imposed by the available computational sources. This is specifically the case for fasted state systems as they were very dilute in bile lipids (6.25 mM in total). Each fasted state system ended up in a single mixed micelle, which grew in size with increasing number of bile lipids while the concentration was kept constant. This behavior is an indication of the above-mentioned situation; i.e., fail to attain the true thermodynamic equilibrium states. As a matter of fact, the true thermodynamic equilibrium state -at the total lipid concentration ranges (6.25–25 mM) and the PL-to-BS ratio (0.25) covered here- is expected to be composed of simple micelles coexisting with minimum-sized mixed micelles as shown by several experimental studies [6,11,12] before. Therefore, due to the fact that the expected phase behavior was not truly obtained in

fasted state systems, the simulations of fasted state should be accepted with caution. The attainment of thermodynamic equilibrium states in dilute systems, in which multiple micellar structures with varying sizes in dynamic equilibrium with free unimers would be observed, requires very large system sizes and long simulation times even with CG force fields [21,53]. Although it is less likely to capture the true equilibrium states via simulations of limited system size and time windows, the results obtained from these simulations still provide valuable insight into the mechanism of micellization. Besides, each micellar structure formed in different sizes can be seen as representative transient state aggregates [54], which appear during the course of digestion and are very dynamic in nature [14,55,56]. These transient state structures are also believed to possess a role in the bioaccesibilities of lipophilic molecules [12,57]. The fate of lipophilic molecules within the aqueous duodenal medium under non-equilibrium conditions would certainly be of interest for further investigations.

In contrast to the fasted state systems, simulations of the fed state system reached a relatively fast convergence with two separate mixed micelles (Fig. 2d). The predicted cluster size distribution in the fed state seems to be more reliable (although not definitive) since a stable phase consisting of more than a single mixed micelle coexisting with simple micelles was obtained. As mentioned above, this is the expected phase behavior of a mixture of PLs and BSs at a total lipid concentration of 25 mM and a PL/BS ratio of 0.25 [6,11,12]. Furthermore, an additional simulation of the system performed in a half-sized simulation box resulted in the same result (data not shown).

The cumulative probability distributions of the aggregation numbers are given in Fig. 3 as block-averaged values over 1 μs increments to analyze the time dependent behaviors. Similar micellization behaviors were observed in all the systems. The initial stages of the simulations were dominated by dimers of cholates and small clusters involving mainly simple micelles, and, to lesser extent small mixed micelles. As the simulations proceeded, these small clusters merged together to form larger aggregates as evidenced by their disappearance towards convergence. For instance, in system C, clusters with small aggregation numbers (3 to 15) dominated the system up to 3 μs. The following 1 μs interval of the trajectory was sampled by relatively larger micelles (with aggregation numbers ranging from 17 to 27) while the smaller aggregates seen in the previous stages were no longer observable, indicating their fusion. Likewise, the largest micelles (37–44) were observed only after the convergence point (4 μs) after which none of the small micelles were observed any more. This finding is also supported by the time evolution of N_w and number of clusters (Fig. 2) values as discussed above. At steady state, the mixed micelles were involved in a dynamic exchange of cholates with the surrounding medium. This was observed by visual inspection of the final stages of the trajectories. It was also observed that once the hydrophobic core was formed by POPC molecules, they never left the micelles. Therefore, we infer that the broadness of the steady state size distributions is due to this dynamic exchange of cholates between the micelles and the aqueous phase. Another observation is that the broadness of the size distribution seems to increase with increasing system size. Taken all together, these observations suggest a mechanism, which is independent of the total bile lipid concentration such that once the hydrophobic core is formed by the POPC tails, cholates try to fill in the available spaces on the micelle's surface. Similar behavior was reported for the self-assembly of mixed micelles composed of cholate and sodium dodecylsulfate [44].

The evolution of micelle formation is demonstrated for the fed state system in Fig. 4 as a collection of subsequent snapshots from the trajectory. The first snapshot (Fig. 4a) displays the initial configuration where all the participant molecules were randomly placed in the box. The fast self-assembly was observed beginning from the earlier stages of the simulation (Fig. 4b). In the course of the simulation, larger micelles were formed by the fusion of smaller clusters (Fig. 4c,d). Moreover, some representative aggregates/micelles formed during the simulation of system A (fasted-8000 nm^3) are given in Fig. 5 to give some idea about the intermolecular interactions. The first aggregates in the earlier stages of the trajectory were formed by the neighboring CHOA (Fig. 5a) and CHOA-POPC (Fig. 5b) molecules. The dimers formed by parallel aligned cholates representing the majority of population, as shown in Fig. 5a, result from the hydrophobic alignment of their steroid backbones. This configuration between bile salts has been reported several times [14,21–24]. Fig. 5b shows a cross alignment of a POPC and a CHOA forming a dimer. This type of arrangement has been also reported between POPC and glycodeoxycholate [28]. The interaction between them is mainly through the hydrophobic side of CHOA and the tails of POPC, as expected. Besides, an electrostatic interaction between the carboxylate and choline moieties of CHOA and POPC, respectively, seems to exist. Imminently, the aggregates became larger by joining of the free cholates. In Fig. 5c, a configuration involving a wrapped POPC tail by three CHOAs is shown. Note that the CHOAs exhibit different alignments with respect to POPC to ensure that the hydrophobic tail beads are effectively shielded from water. The strong affinity between POPC tail beads due to the hydrophobic effects resulted in aggregation of two or a few more POPC molecules during the early stages of simulations. An example arrangement between two POPC molecules aligned antiparallel to each other and a single CHOA trying to cover the tail beads is given in Fig. 5d. In the following time steps, those small aggregates fused in together to form larger clusters. The cluster shown in Fig. 5e, which is composed of 14 molecules in total, was formed by the fusion of the smaller aggregates including the ones in Fig. 5c,d. As the figure suggests, the micelle core is composed of POPC tail segments while the charged head beads protrude from the micelle surface into the aqueous phase. CHOAs, on the other hand, are arranged as wedges in different configurations on the micelle surface such that their hydrophilic sides are facing the solvent while trying to cover the POPC tails with their hydrophobic sides (circled molecule in Fig. 5e). Though, the opposite alignment (hydrophilic side facing the micelle core) was also occasionally possible (dash-circled molecule in Fig. 5e). Their alignment on the micelle surface was mostly flat (although not perfectly) as also suggested by the radial density distributions (RDDs) and the angle calculations (see Section 3.2.2 and 3.2.3). These morphological observations were also reported in other similar computational self-assembly studies involving bile salts and phospholipids [15,16,21,24,58]. Finally, a representative micelle belonging to the production runs is displayed in Fig. 5f. Further findings on the morphological details of the stable mixed micelles are discussed in Section 3.2. Only the micelles with aggregation numbers that exhibit the largest cumulative probability after the convergence point (i.e., 20, 32, 39 and 62 membered micelles for systems A, B, C and D, respectively) were chosen for further analysis (Fig. S1).

3.2. Size dependent structural characterization

3.2.1. Size and shape properties

The radii of gyration (R_g) of the selected micelles were calculated to acquire an idea about the micelle sizes. Experimental studies have shown that micelle size is dependent on the total lipid concentration, the ratio of PL/BS in the medium, and the micellar PL/BS ratio; i.e. the ratio of PL to BS within the micelle [59]. As mentioned before, the PL/BS ratio in solution used in this study is 0.25 regardless of the total concentration, which rules out the assessment of the dependence of micellar properties on this factor. The micellar PL/BS ratios in our steady state micelles and the calculated R_g values are given in Table 2.

We will begin with the analysis of the mixed micelle at fed state (62-Fed) as it is considered to represent the true thermodynamic equilibrium structure fairly (Section 3.1). Its R_g was found to be 1.896 ± 0.016 nm, which is in agreement with the literature. Mazer and coworkers [6] reported that the hydrodynamic radii (R_h) of the mixed micelles changed between 1.8 and 3.5 nm when the PL/BS ratio in solution was smaller than 0.6. Similarly, Kossena et al. [45] reported an R_h value of 3.5 nm for both fasted and fed state mixed micelles where

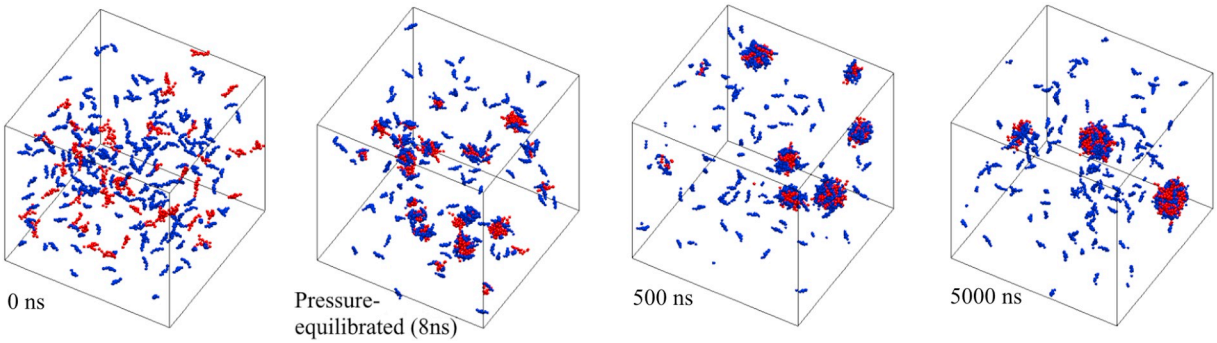

Fig. 4. Snapshots from the trajectory of system D (Fed-16,000 nm^3) showing the evolution of self-assembly. Cholate and POPC molecules are colored in blue and red, respectively. Water molecules and ions are omitted for visual clarity. (For interpretation of the references to colour in this figure legend, the reader is referred to the web version of this article.)

the PL/BS ratio in solution was 0.25. Schurtenberger et al. [60] and Khoshakhlagh et al. [13] determined an R_h of 2.4 nm when that ratio was equal to 0.3 and 0.25, respectively. More recently, Clulow et al. [26] have reported R_h values ranging between 2.5 and 3 nm for fed state mixed micelles, which were prepared at exactly the same total lipids concentration and PL/BS ratio used in this study. For the sake of a fair comparison, one should keep in mind that R_h value for a spheroidal particle is greater than its R_g. More specifically, R_g/R_h ratio is 0.77 for a solid sphere [61]. As will be discussed below, our micelles were found to be slightly ellipsoidal in shape. Therefore, we believe the R_g value determined for the 62-fed micelle reproduces the sizes reported in the literature fairly well.

The calculated R_g values for the fasted state mixed micelles range from 1.301 ± 0.026 nm to 1.653 ± 0.018 nm with increasing aggregation numbers (Table 2). Once more, we should note that the stabilized structures obtained from fasted state systems in this work do not completely characterize the corresponding true thermodynamic equilibrium state due to the limited system size issues (Section 3.1). Indeed, the experimental values reported for the radius of mixed micelles at fasted state concentrations range from 2.6 to 7.5 nm [6,13,26,45,60]. On the other hand, Fatouros et al. [62] reported an R_g of 2.5 ± 0.9 nm for a mixed micelle formed in a 5:1 mM mixture of BS:PL. The differences between the results reported in separate studies might be arising from the different types, amounts or micellar ratios of BS and PL, the experimental conditions and the methods used to determine the size of micelles. The compositions of the selected stable micelles and the dependence of their size on aggregation number (N) were also analyzed (Table 2). Comparison of the fasted state systems suggests that at a fixed total lipids concentration and BS/PL ratio in solution, micelle size increases with increasing micellar POPC/CHOA ratio. Similar behavior was reported for cholate/DPPC mixed micelles by Haustein et al. [24]. The micellar ratio of PL/BS in the 62-fed micelle is also around 0.6. Finally, the R_g was found to be linearly dependent on $N^{1/3}$ (R^2 = 0.9962, Fig. S2-a) as expected for spheroidal micelles.

To characterize the shape of micelles, the ratios of three principal moments of inertia (I_1/I_2 and I_2/I_3) were calculated (where $I_1 \leq I_2 \leq I_3$). The ratios, I_1/I_2 and I_2/I_3, describe the micelle shapes; i.e., for spherical micelles, $I_1 \approx I_2 \approx I_3$ and $I_1/I_2 \approx I_2/I_3 \approx 1$; for disc-like micelles, $I_1 \approx I_2 \ll I_3$, and $I_1/I_2 \approx 1$ and $I_2/I_3 \approx 0$; for rod-like micelles, $I_1 \ll I_2 \approx I_3$, $I_1/I_2 \approx 0$ and $I_2/I_3 \approx 1$. As shown in Table 2, the average values for the ratios are close to, but smaller than 1. This indicates that the micelles are globular; not perfectly sphere, but slightly ellipsoidal in shape. Comparison of the values for each micelle suggests that the micelles are pretty similar in shape. It is only the smallest micelle (20-Fa), which seems to deviate more from spherical geometry. This must be due to the compositional differences rather than the micelle size for two reasons. Firstly, the ratios of the moments of inertia for the three largest micelles are very similar although their sizes are different, indicating no size dependence. Secondly, the micellar POPC/CHOA ratios in those micelles are similar (~0.6) while that of the smallest micelle is distinctive (0.43). Therefore, it must be this compositional difference, which led to a less spherical geometry in the smallest micelle. This behavior was observed also for DPC-CHOA micelles, which were shown to deviate from sphericity to a larger extent with increasing CHOA/DPC ratios [21]. We infer that the dependence of the micelle shape on its composition is a result of its dependently changing flexibility, which is

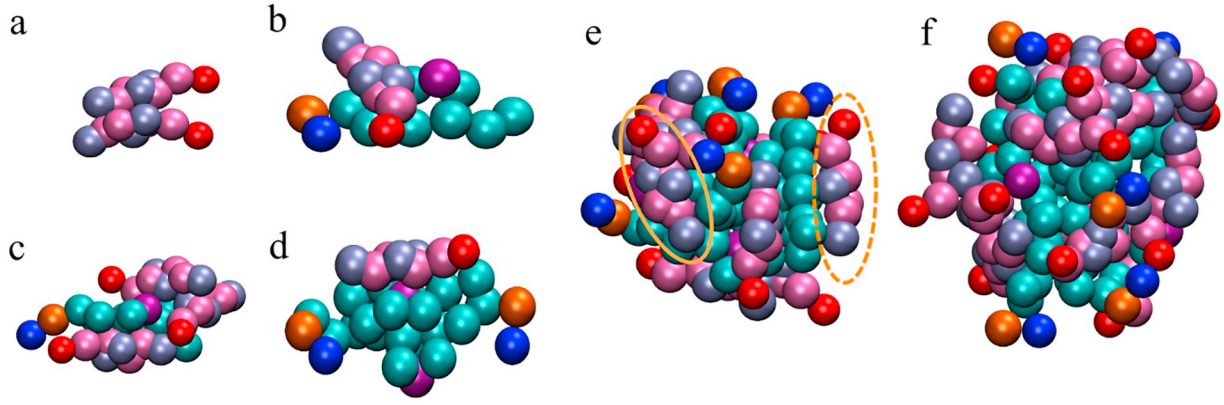

Fig. 5. The representative aggregates that were formed during the simulation of system A (Fasted-8000 nm^3). The hydrophobic, hydrophilic and charged beads of cholates are colored in pink, ice blue and red, respectively. $NC3^+$ beads are colored in blue while $PO4^-$ beads are colored in orange. Glycerol and tail beads of POPCs are colored in cyan except the bead with an intrinsic double bond, which is colored in purple. The representative aggregates 'a', 'b', 'c', 'd' were formed at ~10 ns, 'e' was formed at ~100 ns, and 'f' was formed at ~1.1 μs of the trajectory. (For interpretation of the references to colour in this figure legend, the reader is referred to the web version of this article.)

Table 2
Structural properties of the selected micelles: Radius of gyration (R_g); ratios of the principal moments of inertia, (I_1/I_2) and (I_2/I_3); total solvent accessible surface area (SASA); SASA per surfactant; the ratio of the hydrophilic SASA to hydrophobic SASA (Phi/Pho); and the average palmitoyl and oleoyl tail lengths of POPCs in the micelles.

System –Selected micelle	Numbers of Cholate:POPC molecules	Micellar POPC/ Cholate ratio	R_g (nm)	I_1/I_2	I_2/I_3	Total SASA (nm^2)	SASA per surfactant (nm^2)	Phi/Pho	Average POPC tail lengths (nm)	
									Palmitoyl[a]	Oleoyl[b]
A - 20Fa	14:6	0.43	1.301 ± 0.026	0.841 ± 0.079	0.902 ± 0.047	76.417 ± 3.333	3.821	5.042	1.158 ± 0.052	1.358 ± 0.085
B - 32Fa	20:12	0.6	1.546 ± 0.017	0.884 ± 0.059	0.918 ± 0.040	103.995 ± 3.651	3.250	6.544	1.170 ± 0.037	1.388 ± 0.060
C - 39Fa	24:15	0.625	1.653 ± 0.018	0.888 ± 0.058	0.919 ± 0.040	116.793 ± 4.095	2.995	7.297	1.171 ± 0.033	1.394 ± 0.052
D - 62Fed	40:22	0.55	1.896 ± 0.016	0.886 ± 0.056	0.927 ± 0.036	146.295 ± 4.511	2.360	9.687	1.176 ± 0.027	1.405 ± 0.043

[a] The average palmitoyl tail length was calculated as the average distance between the C1A and C4A beads of POPCs over the corresponding steady state trajectory.
[b] The average oleoyl tail length was calculated as the average distance between the C1B and C5B beads of POPCs over the corresponding steady state trajectory.

a function of the core fluidity. In the next section, we show that the core packing density of the POPC tails is the lowest in the smallest micelle, and increases with micelle size. Thus, the core fluidity is expected to be the highest in the smallest micelle resulting in more flexibility in shape. The latter can be inferred from the higher standard deviations of the corresponding I_1/I_2 and I_2/I_3 ratios in the smallest micelle compared to the others. All these differences prevailing, we should still note that they are small. It remains to be seen whether more significant differences would be observed for micelles covering a larger size range than the one studied in this work.

Another size dependent property is the solvent accessible surface area (SASA). The calculations were performed using a solvent probe of 0.56 nm in radius to mimic one MARTINI water bead, which represents four atomistic water molecules. Table 2 displays the total SASA, SASA per surfactant, and the ratio of the hydrophilic to hydrophobic SASA (Phi/Pho). The total SASA increased with micelle size as expected. For spheroidal micelles, it is expected that the total SASA is related linearly to $N^{2/3}$. This relationship was also observed for the micelles of this work to a good degree ($R^2 = 0.9894$, Fig. S2-b). The small divergence might be due to that the micelles are not perfect spheres and their surfaces are rough (as it is seen in Fig. 4 and Fig. 5e), which also contributes to the calculation of SASA. The contribution of the hydrophobic SASA to the total SASA is very small as it is understood from the high (and ever increasing) Phi/Pho ratios. As a higher Phi/Pho ratio means a more thermodynamically favorable organization of the hydrophilic and hydrophobic domains [54], we can say that as the micelles get larger they become more stable. This can be interpreted as evidence to the notion that hydrophobic effects are the main driving forces for the micellization. Finally, the decrease in total SASA per surfactant with increasing micelle size points to a denser surface packing of the molecules with size. This is also supported by the joint interpretation of the RDDs and angle measurement results (Section 3.2.2 and 3.2.3).

3.2.2. Radial density distributions

The RDDs of selected beads in a molecule with respect to center of mass (com) of the micelles were calculated to gain detailed information about the local inner structures and the distributions of water and ions around them. A general representation of the inner and surface organization of the molecules is depicted in Fig. 6a, which displays the RDDs of the specified moieties of POPC /CHOA, water molecules and ions with respect to the com of the micelle for the 62-Fed system. It shows that the core is occupied solely by POPC tails while CHOAs are located at the micelle surface. Water molecules, which solvate the head groups of CHOA, cannot diffuse into the micelle core. The inset figure shows the close view of the interface region. It is seen that the intermediate glycerol beads (GL) of POPCs are localized at the micelle surface where the water and POPC tail RDDs intersect each other (at 1.96 nm away from the center). The charged head groups ($PO4^-$ and $NC3^+$) protrude from the micelle surface and are in direct contact with water. Their orientation on the surface seems to be somewhat flat since

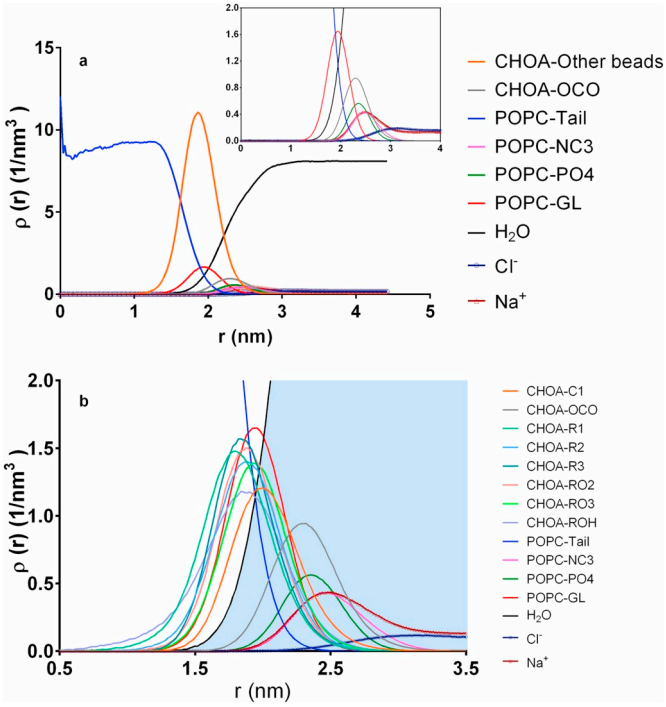

Fig. 6. Radial density distributions (RDDs) (ρ(*r*)) of different moieties of the constituent molecules and ions with respect to center of mass of the micelle for the 62-Fed system. a) RDDs of the specified moieties of CHOA (cholate) and POPC molecules. The close view of the interface region is given in the inset, where all other beads except the OCO^- bead of CHOA are omitted for clarity. b) The close view of the RDDs of the individual beads of CHOA molecules at the interface. RDDs of the surrounding Na^+, Cl^- ions and water (−) molecules are included in both graphs.

the maxima of their RDDs are only ~0.1 nm away from each other. This is apparently smaller than the average distance between the choline and phosphate beads in a single POPC molecule, which was calculated as 0.455 nm. This is also supported by the average angle calculations between the PO4-NC3 vector on a POPC molecule and the micelle's surface normal (Fig. 7a). The protrusion of the negatively charged phosphate groups of POPCs into the aqueous medium is slightly (< 0.1 nm) further than that of the negatively charged carboxylate moieties of CHOAs. The presence of an ionic double layer around the micelle surface is also apparent. The first shell is comprised of Na^+ ions localized around the carboxylate and phosphate moieties of CHOAs and POPCs, respectively, coinciding with the location of $NC3^+$ groups of POPCs. This suggests that the Na^+ ions fill the left over space from the protruding choline moieties of POPCs over the micelle surface, and help in screening the electrostatic repulsion between the negatively charged

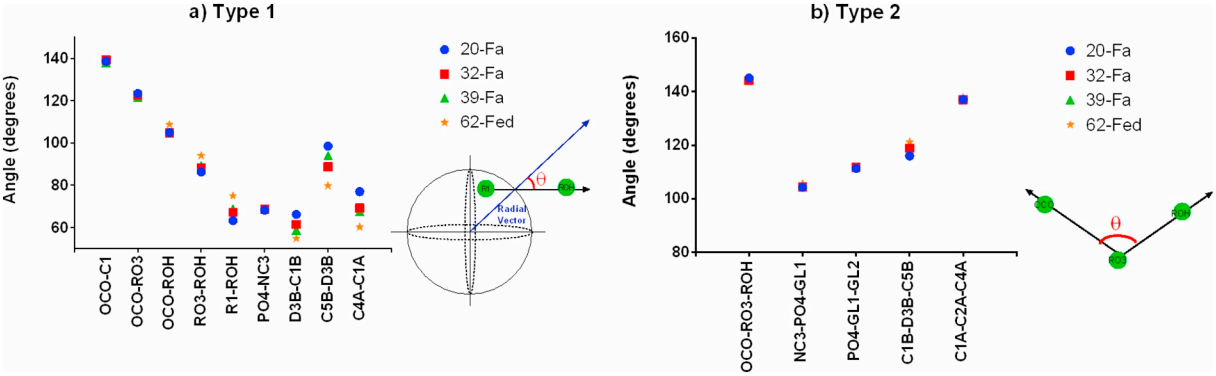

Fig. 7. a) Type I average angles between a vector of two selected beads in a molecule and the local sphere normal (radial vector). The origin of each vector is the first specified bead; hence the direction of each vector is from the first to the second specified bead. The local sphere normal is the vector which connects the com of the micelle to the midpoint of the selected beads' positions as shown in the inset. b) Type II average angles between two vectors in a molecule. The origin of each vector is the middle specified bead; hence the directions of the vectors are from the middle to the end beads as shown in the inset. The selected beads for angle calculations are given in x-axis. (20-Fa: blue dot, 32-Fa: red square, 39-Fa: green triangle, 62-Fed: orange star). (For interpretation of the references to colour in this figure legend, the reader is referred to the web version of this article.)

head groups of CHOAs and POPCs on the surface. The second shell of the double layer is formed by Cl^- ions surrounding the members of the first shell. All of these general features were also reported in the atomistic simulations of Marrink and Mark [16] and Sayyed-Ahmad et al. [21] in which the mixed micelles of POPC-CHOA and DPC-CHOA were characterized, respectively. Therefore, we can say that the internal organizations of BSs and PLs are similar in the mixed micelles regardless of the chemistry. Furthermore, the ability of MARTINI model in reproducing the structural features of dietary mixed micelles is demonstrated once more through this study.

More detailed information about the structuring of CHOAs within the micelle is obtained from Fig. 6b, which shows the RDDs of each CHOA bead with respect to the com of the micelle. It is observed that the peaks corresponding to the beads of the sterol body are located almost at the same distance away from the micelle com except that the beads embodying the methyl groups (R1 and R3) seem to penetrate deeper towards the core. This indicates that the sterol bodies are mainly oriented parallel at the surface with their hydrophilic faces being exposed to the aqueous environment, which is typical in mixed micelles of fully deprotonated bile salts and phospholipids [16,21,24,30,58]. However, the widths of the distributions are not narrow enough to disregard the possibilities of different orientations. Especially, the end hydroxyl group of cholate (ROH bead) shows a wider distribution indicating a deeper penetration inside the micelle. Thus, we can say that the cholates are not always aligned flat on the micelle surface, but, occasionally, are able to adopt different orientations including more perpendicular ones. On the other hand, the RDD of the OCO^- beads depicts a different orientation of the carboxylate groups at the micelle surface. They seem to protrude from the surface into the aqueous environment where they are completely solvated with water. This suggests that the carboxylate side chains of CHOAs are oriented such that they stick out from the surface, which gives a wedge-like shape to the molecules. These findings, which conform to the findings of others [16,21], were also verified by the angle calculations of which the results are given in the next section. Fig. 6b also shows that the beads embodying the methyl groups (R1 and R3) are largely solvated by POPC tails, which reflects the importance of short-ranged van der Waals interactions between these moieties in maintaining the stability of micelles. Additionally, the interaction sites embodying the hydroxyl groups (RO3, RO2, ROH) seem to be located in very close proximity of the glycerol beads of POPCs. This feature was also reported in the atomistic simulations of Marrink and Mark [16], which showed that the hydrogens of the hydroxyl groups of cholates spent substantial amount of their time (30–40%) with forming H-bonds with the carbonyl oxygens of the glycerol moieties of POPC's. Therefore, we can say that although H-bonding is under-represented in the MARTINI force field, associated structural details are yet sufficiently reproduced.

Comparison of the RDDs belonging to the other systems (Fig. S3) indicates that the organization of the constituent molecules, ions and the water molecules within/around a micelle is qualitatively the same regardless of the micelle size or initial concentrations in the solution. Small quantitative discrepancies exist due to the size effects; i.e. the maxima are shifted towards the core and the distributions become narrower as the micelle size decreases. On the other hand, the core packing density seems to be affected by the micelle size and the micellar POPC amounts. This is inferred from the shapes of the RDDs corresponding to the POPC tails, which exhibit marked differences with increasing micelle size. For the smallest micelle (20-Fa), the foregoing RDD has peaks and valleys representing higher and lower density regions, respectively (Fig. S3-a). Especially, the decaying density towards the com of the micelle is worth to mention. Several researchers reported lower densities towards the micelle core due to the steric repulsion of the tail ends, which is typical for phospholipid tails in fluid state [16,63,64]. However, as the micelle size increases the peaks and valleys become less prominent (Fig. S3-b,c), and eventually disappear for the largest micelle (62-Fed, Fig. 6a). This suggests that the core packing gets more uniform with increasing micelle size. The reason behind can be clarified by an approximate calculation of the effective core volume per POPC molecule for each micelle. Assuming all the micelles are perfect spheres and roughly taking the core radius as the average distance between the micelle com and the GL beads of POPCs, we see that the effective core volume per POPC molecule diminishes as the micelle size increases. For instance, the average micelle com-GL bead distance in the smallest and the largest micelles are 1.30 nm, and 1.96 nm, respectively. Based on the aforementioned assumptions, these give effective volumes per POPC of 1.53 nm^3 and 1.43 nm^3 within the micelle core, respectively. Calculations on the intermediate size micelles also conform to the trend. Hence, the packing density of the POPC tails within the micelle core increases with increasing micelle size. Furthermore, below (Section 3.2.3), we also show that the orientation of the tails with respect to the radial vector, and, to lesser extent, the conformations of the oleoyl tails change with micelle size. Therefore, we conclude that the increasing core packing density with increasing micelle size, which causes improved alignment of the tails with the radial direction (and barely more stretched oleoyl tails), results in more uniform distribution of the tails within the core.

3.2.3. *Internal and surface orientations of the molecules*

The average angles between selected vectors in a molecule were calculated to further analyze the internal and surface orientation of the constituent molecules and/or specific moieties. The calculations were

performed considering two different types of angles: Type I: The angle between a vector which is formed by two selected beads on a molecule and the radial vector (calculated as the vector from the com of the micelle to the midpoint of the selected beads' positions) (see inset of Fig. 7a); and Type II: The angle between two vectors in a molecule denoted by 3 beads in total, of which the middle bead is the origin of both vectors and the remaining ones indicate their directions (see inset of Fig. 7b). The latter gives information about the conformations of the molecules within the micelles.

The RDDs (Fig. S3 and Fig. 6) showed that CHOAs are localized at the micelle surface. Therefore, the calculation of the average angle between a specified vector on CHOAs and the radial direction would give information about the alignments of these molecules at the micelle surface. The calculations were performed for the whole CHOA molecule (represented by the vector connecting the OCO^- bead to the ROH bead) as well as for two parts of a molecule, where one part is the sterol body represented by the vector connecting the RO3 bead to ROH, and the remaining part represented by the vector connecting the OCO^- bead to RO3. The alignments of the short hydrophilic tail and the hydroxyl end of the sterol body were investigated separately through the vectors connecting the OCO^- bead to C1, and the R1 to ROH, respectively. The results are given in Fig. 7a for all the systems. Firstly, the average angle between the RO3-ROH vector on a CHOA molecule and the radial vector is observed to be in the range 86–94°, which suggests that the sterol bodies of the cholates are primarily oriented parallel to the micelle surface. This was inferred from the RDDs as well. This result is also consistent with those of several experimental studies [65–68], which showed that bile salts preferably sit parallel to the PL-water interface, because highly ordered PL interfaces do not allow BSs to penetrate deep into the mono/bilayer as this would lead to a large disorder in the structure. On the other hand, the BSs are known to exhibit the opposite behavior at hydrocarbon-water interfaces [69,70]. The contradiction is attributed to the differences between the structural differences between the two surfaces. Since the hydrocarbon interfaces like octanol or decane are already disordered, they allow BSs to penetrate deep without being disrupted significantly [70]. That being said, the broad distributions (RDDs) also suggested that the molecules adopted more perpendicular orientations occasionally. This finding is also supported by the histograms of the observed angles between the vectors R1-ROH (or RO3-ROH) and the radial vector (Fig. S4-a,b). Furthermore, the charged hydrophilic halves of CHOAs seem to adopt a tilted orientation with respect to the radial direction, which is inferred from the average angle between the OCO-RO3 vector and the radial vector (~120°). The average observed angle between the protruding short tail (OCO-C1) and the radial vector was also found to be ~140° regardless of the micelle size. All of these results together with the intramolecular average Type II angle values given in Fig. 7b (~145° for OCO-RO3-ROH) suggest that the shape of the CHOA molecules is wedge-like with their sterol body aligned more or less parallel at the surface and their hydrophilic tail protruding into the aqueous environment with a tilt of ~50° from the surface. Similar findings were reported in resembling studies as well [16,21,24]. Finally, it is observed that the orientation of CHOAs changes slightly with increasing micelle size. This is inferred from the increasing angles between the vectors OCO^-ROH, RO3-ROH, R1-ROH and the radial vector with growing micelle size (Fig. 7a), which indicate that as the micelles get larger the CHOAs are sampling more perpendicular orientations with respect to the micelle surface. This might be a consequence of the decreasing surface area per surfactant with increasing micelle size (see Table 2); i.e. increased packing density at the micelle surface.

Regarding the orientation of the head groups of POPCs at the surface, we can say that the findings from the RDDs are supported by Type I angle results. The average angle between the PO4-NC3 vector in a POPC molecule and the radial vector was found to be ~68° regardless of the micelle size (Fig. 7a), which indicates that the protruding head groups are principally aligned almost flat on the micelle surface. This type of orientation of the phosphate-choline head groups at the surface was also reported for simple micelles composed of lysophospholipids [42]. Nevertheless, the angle distribution histogram shows that miscellaneous orientations were practically possible (Fig. S4-c). Fig. 7a also gives idea about the average orientations of the palmitoyl and the oleoyl tails of POPCs with respect to the radial direction. First of all, it is clear that the tails are not perfectly aligned with the radial direction as it was proposed by the classical idealized micelle models. Indeed, the disordered nature of the surfactant tails (in different types of micelles) has been demonstrated several times by MD simulations [16,22,44,63]. It is clear that the orientations of the upper (D3B-C1B) and the lower (C5B-D3B) parts of the oleoyl tails are significantly different indicating the presence of a kick in the tail as expected due to the inherent double bond. Specifically, the average angle intrinsic to the oleoyl tail due to the kick (Type II C1B-D3B-C5B angle) was found to be around 120° (Fig. 7b). On the other hand, the angle distribution histogram shows that more bent or elongated conformations were also occasionally adopted (Fig. S5-a). Moreover, the distribution in the smallest micelle (20-Fa) exhibits a small shift towards lower angles (Fig. S5-a). This, (as well as the decreasing average Type II C1B-D3B-C5B angles (Fig. 7b) and the decreasing oleoyl tail lengths in the core (the average distance between the C1B and C5B beads in a POPC molecule- see Table 2) with diminishing micelle size, indicate that the oleoyl tails of the POPCs are able to retain slightly more kinked conformations as the micelles get smaller. This must be due to the weakened packing constraints within the core with decreasing micelle size as discussed above in Section 3.2.2. In other words, each oleoyl tail has slightly more space to freely sample more kinked conformations as the effective volume per molecule within the core was found to increase with diminishing micelle size. Speaking of the palmitoyl tails, they seem to have sampled more stretched conformations compared to the oleoyl tails as the average C1A-C2A-C4A angle values (135°, Fig. 7b) suggest. However, we cannot speak of any remarkable conformational change in palmitoyl tails with increasing micelle size since there is no evidence for such a change in the Type II C1A-C2A-C4A angle distribution histograms (Fig. S5-b). Besides, the increase in the average tail length (the average distance between the C1A and C4A beads in a POPC molecule- see Table 2) with growing micelle size is very low (lower than 0.02 nm) to take into consideration. Another significant outcome from Fig. 7a is that although the tails of POPCs are not perfectly aligned along the radial direction, they become more capable of doing so as the micelles get larger. This is inferred from the diminishing average angles between the vectors D3B-C1B, C5B-D3B, C4A-C1A and the radial vector with increasing micelle size. This feature is even more significant in the corresponding angle distribution histograms, which exhibit marked shifts to lower angles with increasing size (Fig. S4-d, e, f). Considering the above-mentioned observations on the intramolecular (Type II) angle distributions belonging to the tails and the average tail lengths, we can say that the increased alignment of POPC tails with radial direction is mainly due to their reorientation within the core imposed by the diminishing effective core volume per POPC molecule with increasing micelle size. The contribution of the slight extension of the oleoyl tails with increasing micelle size is thought to be minimal when the extent of increase in the tail length is taken into account. The improved alignment of both of the tails also resulted in denser and more uniform packing in the core as discussed before (Section 3.2.2). Though, the fluid nature of the core was not lost as the broadness of the distributions indicates (Fig. S5-a, b). Finally, regardless of the micelle size, the distribution of the intramolecular NC3-PO4-GL1 angle was found to be bimodal (giving peaks at ~60° and ~110°) (Fig. S5-c), while the PO4-GL1-GL2 angle distribution was unimodal giving a peak at ~110° (Fig. S5-d).

3.2.4. Discussion in the context of previously proposed mixed micelle models

A few hypothetical models describing the structure of mixed micelles composed of BSs and PLs have been previously proposed in the literature. The earliest model of Small [71], which was based on X-ray diffraction experiments, proposed a disk-like shape. The model assumed

that BS molecules surrounded a disk-like portion of a lecithin bilayer on its perimeter with their hydrophilic sides facing the aqueous environment and the hydrophobic sides interacting with the PL tails [6]. However, its quantitative predictions have never been satisfactorily verified by experiments [6,72]. Mazer et al. [6,73,74] proposed an improved version of the disk model such that H-bonded dimers of BSs were also incorporated in high concentrations within the PL bilayer as well as they were located at its perimeter. The same group, however, later found out that the data were, in fact, in excellent agreement with a worm-like mixed micelle model [8]. As a matter of fact, it has long after been suggested through time-resolved light and neutron scattering experiments that disk-like micelles were just the transition structures before vesicle formation on sudden dilution of spherical or rod-like micelles [75,76]. Shankland [77] proposed a stacked-disk model to describe rod-like mixed micelles. He envisaged that several disk-like micelles were stacked on top of each other with the polar head groups facing each other and a thin water layer in between. However, Ulmius et al. [65] proposed an alternative, the so-called radial-shell model, to describe the internal structure of infinite rod-like micelles, which stack side by side to form the hexagonal liquid-crystalline phases of cholate-lecithin-water ternary system. Their model involved organization of the molecules in a cylinder (rod) such that PL head groups were placed at the cylinder surface with the tails pointing radially towards the rod axis, while BSs either lied flatly on the surface or penetrated deeper into the rod with their charged head groups on the surface. Finally, Nichols and Ozarowski [59] proposed the capped-rod model, which was based on the radial-shell model, in which the arrangements of PLs and BSs in the rod were the same as described above, but the ends of the rods were covered by BS-rich caps and the orientation of the BSs on the rod surface was mostly flat. Since then, there have been several experimental [7,8,10,11,78,79] and computational [16,21,24,26–29] studies endorsing the radial-shell arrangements of BSs and PLs in mixed micelles.

Based on the given information, the results of our structural analyses lead us to the assessment that the radial-shell model of Ulmius et al. [65] and Nichols and Ozarowski [59] best describes the morphology of our mixed micelles despite the fact that our micelles are not rod-like, but slightly ellipsoidal in shape. So far, many experimental studies [2,6–8,59,60,71,72,80,81] have shown that mixed micelle size and shape are strongly influenced by total lipids concentration and PL/BS ratio in solution. The commonly accepted belief is that the structure changes from a mixture of spherical mixed and simple micelles to rod-like mixed micelles, and finally to vesicles as the medium is diluted [76]. On the other hand, at a fixed total lipids concentration, the shape transforms from spherical to elongated rods as the PL/BS ratio increases [8]. To the best of our knowledge, there is only a single experimental work [26] in the literature, exactly addressing the total lipids concentrations (6.25 mM (0.3 g/dL) - 25 mM (1.2 g/dL)) and PL/BS ratio (0.25) adopted in this study. Clulow et al. [26] have recently characterized in-house prepared sodium taurodeoxycholate-DOPC mixed micelles at fed and fasted state concentrations using small-angle X-ray scattering (SAXS), dynamic light scattering and cryo-transmission electron microscopy (cryo-TEM). They did not observe any rod-like structures, but showed that all the micelles were oblate ellipsoids irrespective of the lipids concentration, conforming to our results. Their findings were also supported by coarse-grained MD simulations in the same study. Although no other experimental study is available to benefit for a direct comparison with our systems, a comparison with the findings of others who have worked within the same region of the BS-PL-water ternary phase diagram (mixture of simple and mixed micelles) is possible. For instance, Hjelm et al. [2] determined via small-angle neutron scattering (SANS) that, at a total lipids concentration of 1 g/dL, the shape of mixed micelles was transformed from long rods to prolate ellipsoids as the PL/BS ratio decreased from 0.9 to 0.56. Although a ratio lower than 0.56 was not experimented in this study, the direction of shape transformation suggests that spheroidal mixed micelles would be observed at lower PL/BS ratios, conforming to our results. This is because BSs have a larger spontaneous curvature than PLs, thus increasing their relative amount forces the aggregates to adopt more curved structures [11,82]. Another study has demonstrated the existence of spheroidal mixed micelles at a total lipids concentration of 20 mM with PL/BS = 0.82 via cryo-TEM [83]. They also stated (the data were not shown) that the images were similar to those of spheroidal mixed micelles observed at higher relative BS concentrations. Moreover, a recent study has shown that spherical micelles were observed at 16 mM total lipids concentration with PL/BS = 0.6 [81].

As a final remark, reminding that we were unable to reproduce the expected phase behavior under fasted state conditions due to limited system size issues, it is possible to question whether or not simulations of a much larger system would give rod-like mixed micelles as suggested by some of the available SAXS or quasi-elastic light scattering (QELS) data gathered under somewhat similar conditions. However, one should keep in mind that the size and shape data interpreted from those techniques are extremely model dependent and subject to error especially if the samples are polydisperse [83]. On the other hand, the recent supportive findings of Clulow et al. [26] obtained both by experiments and MD simulations give us a measure of confidence that our simulations capture the basic features of the morphology of mixed micelles also at fasted state.

4. Conclusions

The aims of the present study were to investigate the evolution of mixed micelle formation under physiological conditions in duodenum both at fasted and fed states and to analyze the structural properties of the steady state micelles as a function of size through coarse-grained molecular dynamics simulations. Cholate and POPC were used as model bile lipids. The analysis of the self-assembly processes showed that the micellization behavior was the same regardless of the total concentration of the bile lipids except that the convergence of the simulation was achieved the fastest under fed state concentrations. The spontaneous aggregations between the neighboring molecules were observed soon after the simulations were started. The initial stages were dominated by dimers of cholates and small clusters, which were principally simple micelles. During the course of the process, the small aggregates fused to form larger ones until stable mixed micelles were attained. It was observed that once the hydrophobic core was formed by POPC molecules they never left the micelle, thereafter which the micelle growth was continued only by the addition of unimers or dimers of cholates. Cholates were continuously involved in a dynamic exchange between the micelles and the aqueous medium, which was responsible for the broadness of the size distributions. The expected phase behavior of the coexistence of multiple mixed micelles with simple micelles and free cholates was attained at the end of fed state simulations only, which denotes a fair representation of the true thermodynamic equilibrium under fed state conditions. Despite the use of a CG model, the prohibitively limited time and length scales sampled were not sufficient to attain a representative true thermodynamic equilibrium system under fasted state concentrations. Therefore, a complete comparison of the structures in both states was not possible. However, considering that the micellization behavior and the general aspects of the micelle morphologies were found to be independent of the total lipids concentration, the steady state micelles obtained in varying sizes in this study can be considered as transient structures that are formed in the duodenum under both fasted and fed states.

The structural analysis revealed that all of the micelles were slightly ellipsoidal regardless of the initial concentration. The shape was found to be dependent on the micellar composition rather than the size. The lower the micellar POPC/cholate ratio, the more flexibility in shape (resulting in rougher surfaces) and the more deviation from the spherical geometry were observed. The size of the micelle obtained under fed state conforms to the experimental data from literature. The R_g was found to be linearly dependent on the (1/3)th power of the aggregation

number as expected for spheroidal micelles. The high and ever increasing ratios of the hydrophilic to hydrophobic SASAs indicate that thermodynamically more favorable organizations of molecules were attained with increasing micelle size. Furthermore, the decrease in the total SASA per surfactant with increasing micelle size indicates a denser surface packing of the molecules.

The internal structures of the micelles were investigated by the help of RDDs and specific angle calculations. The general aspects of the morphology were found to be the same regardless of the total lipids concentration and micelle size. The previously proposed radial-shell model best describes the structure of the micelles. The general picture is such that the core is composed of POPC tails, the glycerol moieties lie on the surface and the charged phosphate and choline groups protrude from the surface to the surrounding medium where they are completely solvated with water. The cholates are located on the surface acting as wedges between the head groups of POPCs with their hydrophobic faces primarily pointing towards the core. Their shape is wedge-like with their sterol backbones aligned more or less flat on the surface and the charged short tails protruding into the aqueous environment with a tilt from the surface. The micelles are surrounded by an ionic double shell of which the inner and the outer ones are constituted by Na^+ and Cl^- ions, respectively. Overall, the structures are flexible and the bile lipids behave as in fluid state as suggested by the broadness of the RDDs and the angle distributions. The comparison of our results with those of other studies conducted with different bile lipids in the literature suggests that the morphologies of the duodenal mixed micelles are similar regardless of the chemistry. On the other hand, our results suggest that small differences might be observed for micelles of varying sizes due to changing packing constraints. For instance, the cholates were shown to sample slightly more perpendicular orientations at the surface with growing micelle size, which was attributed to the increasing packing density of the molecules at the surface. Besides, the core packing density of the POPC tails was found to increase with micelle size. The main consequence was an improvement in the alignments of POPC tails with radial direction. The overall effect was a more uniform density in the micelle core with increasing size. Whether or not more significant structural variations would be observed for micelles covering a larger size range than the one studied in this work remains to be seen.

The information gained by this study sheds light on the mixed micelle formation in the duodenum under physiologically relevant concentrations and the morphology of the micelles at molecular level. The effects of the presence of different types of lipid digestion products (fatty acids) to the formation mechanism and the micelle structure are under study. The outcomes of these studies are expected to be utilized in the design of effective delivery systems for poorly absorbed drugs and nutraceuticals.

Acknowledgements

Computing resources used in this work were provided partially by TUBITAK ULAKBIM, High Performance and Grid Computing Center (TRUBA resources), and the National Center for High Performance Computing of Turkey (UHEM) under grant number 5004012016. IZTECH is greatly acknowledged for the financial support under the grant number 2016İYTE19.

Appendix A. Supplementary data

Supplementary data to this article can be found online at https://doi.org/10.1016/j.bpc.2019.02.001.

References

[1] S. Rozner, D.E. Shalev, A.I. Shames, M.F. Ottaviani, A. Aserin, N. Garti, Do food microemulsions and dietary mixed micelles interact? Colloids Surf. B: Biointerfaces 77 (2010) 22–30, https://doi.org/10.1016/j.colsurfb.2009.12.026.

[2] R.P. Hjelm, M.H. Alkan, P. Thiyagarajan, Small-angle neutron scattering studies of mixed bile salt-lecithin colloids, Mol. Cryst. Liq. Cryst. Inc. Nonlinear Opt. (1990), https://doi.org/10.1080/00268949008025796.

[3] T.L. Lin, S.H. Chen, N.E. Gabriel, M.F. Roberts, Use of small-angle neutron scattering to determine the structure and interaction of dihexanoylphosphatidylcholine micelles, J. Am. Chem. Soc. 108 (1986) 3499–3507, https://doi.org/10.1021/ja00272a055.

[4] O. Rezhdo, S. Di Maio, P. Le, K.C. Littrell, R.L. Carrier, S.-H. Chen, Characterization of colloidal structures during intestinal lipolysis using small-angle neutron scattering, J. Colloid Interface Sci. 499 (2017) 189–201, https://doi.org/10.1016/j.jcis.2017.03.109.

[5] H. Aizawa, S. Ichikawa, E. Kotake-Nara, A. Nagao, Effects of a lysophosphatidylcholine and a phosphatidylcholine on the morphology of taurocholic acid-based mixed micelles as determined by small-angle X-ray scattering, J. Dispers. Sci. Technol. (2017) 1–7, https://doi.org/10.1080/01932691.2017.1380529.

[6] N.A. Mazer, G.B. Benedek, M.C. Carey, Quasielastic light-scattering studies of aqueous biliary lipid systems. Mixed micelle formation in bile salt-lecithin solutions, Biochemistry. 19 (1980) 601–615, https://doi.org/10.1021/bi00545a001.

[7] R.P. Hjelm, P. Thiyagarajan, H. Önyüksel, Organization of phosphatidylcholine and bile salt in rodlike mixed micelles, J. Phys. Chem. 96 (1992) 8653–8661, https://doi.org/10.1021/j100200a080.

[8] D.E. Cohen, G.M. Thurston, R.A. Chamberlin, G.B. Benedek, M.C. Carey, Laser light scattering evidence for a common wormlike growth structure of mixed micelles in bile salt- and straight-chain detergent- phosphatidylcholine aqueous systems: relevance to the micellar structure of bile, Biochemistry. 37 (1998) 14798–14814, https://doi.org/10.1021/bi980182y.

[9] A. Hildebrand, R. Neubert, P. Garidel, A. Blume, Bile salt induced solubilization of synthetic phosphatidylcholine vesicles studied by isothermal titration calorimetry, Langmuir. 18 (2002) 2836–2847, https://doi.org/10.1021/la011421c.

[10] L. Arleth, D. Roskilde, S.U. Egelhaaf, P. Schurtenberger, J.S. Pedersen, Growth Behavior of Mixed Wormlike Micelles: A Small-Angle Scattering Study of the Lecithin - Bile Salt System, (2003), pp. 4402–4410.

[11] D. Madenci, A. Salonen, P. Schurtenberger, J.S. Pedersen, S.U. Egelhaaf, Simple model for the growth behaviour of mixed lecithin-bile salt micelles, Phys. Chem. Chem. Phys. 13 (2011) 3171–3178, https://doi.org/10.1039/c0cp01700k.

[12] W.A. Birru, D.B. Warren, A. Ibrahim, H.D. Williams, H. Benameur, C.J.H. Porter, D.K. Chalmers, C.W. Pouton, Digestion of phospholipids after secretion of bile into the duodenum changes the phase behavior of bile components, Mol. Pharm. 11 (2014) 2825–2834, https://doi.org/10.1021/mp500193g.

[13] P. Khoshakhlagh, R. Johnson, T. Nawroth, P. Langguth, L. Schmueser, N. Hellmann, H. Decker, N.K. Szekely, Nanoparticle structure development in the gastro-intestinal model fluid FaSSIF mod6.5 from several phospholipids at various water content relevant for oral drug administration, Eur. J. Lipid Sci. Technol. 116 (2014) 1155–1166, https://doi.org/10.1002/ejlt.201400066.

[14] D. Madenci, S.U. Egelhaaf, Self-assembly in aqueous bile salt solutions, Curr. Opin. Colloid Interface Sci. 15 (2010) 109–115, https://doi.org/10.1016/j.cocis.2009.11.010.

[15] P. Prakash, A. Sayyed-Ahmad, Y. Zhou, D.E. Volk, D.G. Gorenstein, E. Dial, L.M. Lichtenberger, A.A. Gorfe, Aggregation behavior of ibuprofen, cholic acid and dodecylphosphocholine micelles, Biochim. Biophys. Acta Biomembr. 1818 (2012) 3040–3047, https://doi.org/10.1016/j.bbamem.2012.07.029.

[16] S.J. Marrink, A.E. Mark, Molecular Dynamics Simulations of Mixed Micelles Modeling Human Bile †, (2002), pp. 5375–5382.

[17] D.B. Warren, D.K. Chalmers, K. Hutchison, W. Dang, C.W. Pouton, Molecular dynamics simulations of spontaneous bile salt aggregation, Colloids Surf. A Physicochem. Eng. Asp. 280 (2006) 182–193, https://doi.org/10.1016/j.colsurfa.2006.02.009.

[18] L.B. Pártay, P. Jedlovszky, M. Sega, Molecular aggregates in aqueous solutions of bile acid salts. Molecular dynamics simulation study, J. Phys. Chem. B 111 (2007) 9886–9896, https://doi.org/10.1021/jp072974k.

[19] L.B. Pártay, M. Sega, P. Jedlovszky, Morphology of bile salt micelles as studied by computer simulation methods, Langmuir. 23 (2007) 12322–12328, https://doi.org/10.1021/la701749u.

[20] L.B. Pârtay, M. Sega, P. Jedlovszky, Counterion binding in the aqueous solutions of bile acid salts, as studied by computer simulation methods, Langmuir. 24 (2008) 10729–10736, https://doi.org/10.1021/la801352d.

[21] A. Sayyed-Ahmad, L.M. Lichtenberger, A.A. Gorfe, Structure and dynamics of cholic acid and dodecylphosphocholine-cholic acid aggregates, Langmuir. 26 (2010) 13407–13414, https://doi.org/10.1021/la102106t.

[22] D.C. Turner, F. Yin, J.T. Kindt, H. Zhang, Molecular dynamics simulations of glycocholate-oleic acid mixed micelle assembly, Langmuir. 26 (2010) 4687–4692, https://doi.org/10.1021/la903573m.

[23] A.V. Verde, D. Frenkel, Simulation study of micelle formation by bile salts, Soft Matter 6 (2010) 3815, https://doi.org/10.1039/c0sm00011f.

[24] M. Haustein, P. Schiller, M. Wahab, H.-J. Mögel, Computer simulations of the formation of bile salt micelles and bile salt/DPPC mixed micelles in aqueous solutions, J. Solut. Chem. 43 (2014) 1755–1770, https://doi.org/10.1007/s10953-014-0239-3.

[25] A. Vila Verde, D. Frenkel, Kinetics of formation of bile salt micelles from coarse-grained Langevin dynamics simulations, Soft Matter 12 (2016) 5172–5179, https://doi.org/10.1039/C6SM00763E.

[26] A.J. Clulow, A. Parrow, A. Hawley, J. Khan, A.C. Pham, P. Larsson, C.A.S. Bergström, B.J. Boyd, Characterization of solubilizing nanoaggregates present in different versions of simulated intestinal fluid, J. Phys. Chem. B 121 (2017) 10869–10881, https://doi.org/10.1021/acs.jpcb.7b08622.

[27] S.J. Marrink, Molecular dynamics simulation of cholesterol nucleation in mixed micelles modelling human bile, Proc. Falk Symp. 139 (2004) 98–105.

[28] W.A. Birru, D.B. Warren, S.J. Headey, H. Benameur, C.J.H. Porter, C.W. Pouton, D.K. Chalmers, Computational models of the gastrointestinal environment. 1. The effect of digestion on the phase behavior of intestinal fluids, Mol. Pharm. 14 (2017)

566–579, https://doi.org/10.1021/acs.molpharmaceut.6b00888.
[29] A.A. Markina, V.A. Ivanov, P.V. Komarov, A.R. Khokhlov, S.H. Tung, Self-assembly of lecithin and bile salt in the presence of inorganic salt in water: mesoscale computer simulation, J. Phys. Chem. B 121 (2017) 7878–7888, https://doi.org/10.1021/acs.jpcb.7b04566.
[30] E.J.A. Suys, D.B. Warren, C.J.H. Porter, H. Benameur, C.W. Pouton, D.K. Chalmers, Computational models of the intestinal environment. 3. The impact of cholesterol content and pH on mixed micelle colloids, Mol. Pharm. 14 (2017) 3684–3697, https://doi.org/10.1021/acs.molpharmaceut.7b00446.
[31] M. Poša, QSPR study of the effect of steroidal hydroxy and oxo substituents on the critical micellar concentration of bile acids, Steroids. 76 (2011) 85–93, https://doi.org/10.1016/j.steroids.2010.09.003.
[32] S.M. Grundy, A.L. Metzger, A physiological method for estimation of hepatic secretion of biliary lipids in man, Gastroenterology. 62 (1972) 1200–1217, https://doi.org/10.1016/S0016-5085(72)80089-1.
[33] M.D. Wilson, L.L. Rudel, Review of cholesterol absorption with emphasis on dietary and biliary cholesterol, J. Lipid Res. 35 (1994) 943–955.
[34] K. Matsuoka, E. Rie, S. Yui, C. Honda, K. Endo, Competitive solubilization of cholesterol and??-sitosterol with changing biliary lipid compositions in model intestinal solution, Chem. Phys. Lipids 165 (2012) 7–14, https://doi.org/10.1016/j.chemphyslip.2011.10.004.
[35] F.M. Coreta-Gomes, W.L.C. Vaz, E. Wasielewski, C.F.G. Geraldes, M.J. Moreno, Quantification of cholesterol solubilized in dietary micelles: dependence on human bile salt variability and the presence of dietary food ingredients, Langmuir. 32 (2016) 4564–4574, https://doi.org/10.1021/acs.langmuir.6b00723.
[36] K. Matsuoka, M. Maeda, Y. Moroi, Characteristics of conjugate bile salt–phosphatidylcholine–cholesterol–water systems, Colloids Surf. B: Biointerfaces 33 (2004) 101–109, https://doi.org/10.1016/j.colsurfb.2003.09.002.
[37] S. Marrink, A. De Vries, A. Mark, Coarse grained model for semiquantitative lipid simulations, J. Phys. Chem. B (2004) 750–760, https://doi.org/10.1021/jp036508g.
[38] S.J. Marrink, D.P. Tieleman, Perspective on the Martini model, Chem. Soc. Rev. 42 (2013) 6801, https://doi.org/10.1039/c3cs60093a.
[39] S.J. Marrink, H.J. Risselada, S. Yefimov, D.P. Tieleman, A.H. De Vries, The MARTINI Force Field: Coarse Grained Model for Biomolecular Simulations the MARTINI Force Field: Coarse Grained Model for Biomolecular Simulations, vol. 111, (2007), pp. 7812–7824, https://doi.org/10.1021/jp071097f.
[40] C.A. López, Z. Sovova, F.J. Van Eerden, A.H. De Vries, S.J. Marrink, Martini force field parameters for glycolipids, J. Chem. Theory Comput. 9 (2013) 1694–1708, https://doi.org/10.1021/ct3009655.
[41] S.O. Yesylevskyy, L.V. Schäfer, D. Sengupta, S.J. Marrink, Polarizable water model for the coarse-grained MARTINI force field, PLoS Comput. Biol. 6 (2010) 1–17, https://doi.org/10.1371/journal.pcbi.1000810.
[42] P. Brocos, P. Mendoza-Espinosa, R. Castillo, J. Mas-Oliva, Á. Piñeiro, Multiscale molecular dynamics simulations of micelles: coarse-grain for self-assembly and atomic resolution for finer details, Soft Matter 8 (2012) 9005, https://doi.org/10.1039/c2sm25877c.
[43] R. Xu, Z. Wang, H. Li, X. He, Dynamics of micelle formation from mixed lipid droplets, Chinese, J. Chem. Phys. 26 (2013) 203, https://doi.org/10.1063/1674-0068/26/02/203-210.
[44] B. Jójárt, M. Poša, B. Fiser, M. Szori, Z. Farkaš, B. Viskolcz, Mixed micelles of sodium cholate and sodium dodecylsulphate 1:1 binary mixture at different temperatures - experimental and theoretical investigations, PLoS ONE 9 (2014) 1–9, https://doi.org/10.1371/journal.pone.0102114.
[45] G.A. Kossena, B.J. Boyd, C.J.H. Porter, W.N. Charman, Separation and characterization of the colloidal phases produced on digestion of common formulation lipids and assessment of their impact on the apparent solubility of selected poorly water-soluble drugs, J. Pharm. Sci. 92 (2003) 634–648, https://doi.org/10.1002/jps.10329.
[46] L. Sek, C.J.H. Porter, A.M. Kaukonen, W.N. Charman, Evaluation of the in-vitro digestion profiles of long and medium chain glycerides and the phase behaviour of their lipolytic products, J. Pharm. Pharmacol. 54 (2002) 29–41, https://doi.org/10.1211/0022357021771896.
[47] T. Schersten, Formation of lithogenic bile in man, Digestion. 9 (1973) 540–553.
[48] S.J. Marrink, H.J. Risselada, S. Yefimov, D.P. Tieleman, A.H. De Vries, The MARTINI force field: coarse grained model for biomolecular simulations, J. Phys. Chem. B 111 (2007) 7812–7824, https://doi.org/10.1021/jp071097f.
[49] B. Hess, C. Kutzner, D. Van Der Spoel, E. Lindahl, GRGMACS 4: algorithms for highly efficient, load-balanced, and scalable molecular simulation, J. Chem. Theory Comput. 4 (2008) 435–447, https://doi.org/10.1021/ct700301q.
[50] H.J.C. Berendsen, J.P.M. Postma, W.F. Van Gunsteren, A. Dinola, J.R. Haak, Molecular dynamics with coupling to an external bath, J. Chem. Phys. 3684 (1984), https://doi.org/10.1063/1.448118.
[51] W. Humphrey, A. Dalke, K. Schulten, VMD: visual molecular dynamics, J. Mol. Graph. 14 (1996) 33–38, https://doi.org/10.1016/0263-7855(96)00018-5.
[52] J.F. Kraft, M. Vestergaard, B. Schiøtt, L. Thøgersen, Modeling the self-assembly and stability of DHPC micelles using atomic resolution and coarse grained MD simulations, J. Chem. Theory Comput. 8 (2012) 1556–1569, https://doi.org/10.1021/ct200921u.
[53] S.A. Sanders, A.Z. Panagiotopoulos, Micellization behavior of coarse grained surfactant models, J. Chem. Phys. 132 (2010), https://doi.org/10.1063/1.3358354.
[54] S. Lebecque, J.-M. Crowet, M.N. Nasir, M. Deleu, L. Lins, Molecular dynamics study of micelles properties according to their size, J. Phys. Chem. B 72 (2017) 6–15, https://doi.org/10.1016/j.jmgm.2016.12.007.
[55] S. Phan, S. Salentinig, E. Gilbert, T.A. Darwish, A. Hawley, R. Nixon-Luke, G. Bryant, B.J. Boyd, Disposition and crystallization of saturated fatty acid in mixed micelles of relevance to lipid digestion, J. Colloid Interface Sci. 449 (2015) 160–166, https://doi.org/10.1016/j.jcis.2014.11.026.
[56] X. Xie, J.M. Cardot, G. Garrait, V. Thery, M. El-Hajji, E. Beyssac, Micelle dynamic simulation and physicochemical characterization of biorelevant media to reflect gastrointestinal environment in fasted and fed states, Eur. J. Pharm. Biopharm. 88 (2014) 565–573, https://doi.org/10.1016/j.ejpb.2014.05.020.
[57] M. Yao, H. Xiao, D.J. McClements, Delivery of lipophilic bioactives: assembly, disassembly, and reassembly of lipid nanoparticles, Annu. Rev. Food Sci. Technol. 5 (2014) 53–81, https://doi.org/10.1146/annurev-food-072913-100350.
[58] W.A. Birru, D.B. Warren, S. Han, H. Benameur, C.J.H. Porter, C.W. Pouton, D.K. Chalmers, Computational models of the gastrointestinal environment. 2. Phase behavior and drug Solubilization capacity of a type I lipid-based drug formulation after digestion, Mol. Pharm. 14 (2017) 580–592, https://doi.org/10.1021/acs.molpharmaceut.6b00887.
[59] J.W. Nichols, J. Ozarowski, Sizing of lecithin-bile salt mixed micelles by size-exclusion high-performance liquid chromatography, Biochemistry. 29 (1990) 4600–4606, https://doi.org/10.1021/bi00471a014.
[60] P. Schurtenberger, N. Mazer, W. Känzig, Micelle to vesicle transition in aqueous solutions of bile salt and lecithin, J. Phys. Chem. 89 (1985) 1042–1049, https://doi.org/10.1021/j100252a031.
[61] B.M. Tande, N.J. Wagner, M.E. Mackay, C.J. Hawker, M. Jeong, Viscosimetric, hydrodynamic, and conformational properties of dendrimers and dendrons, Macromolecules. 34 (2001) 8580–8585, https://doi.org/10.1021/ma011265g.
[62] D.G. Fatouros, B. Bergenstahl, A. Mullertz, Morphological observations on a lipid-based drug delivery system during in vitro digestion, Eur. J. Pharm. Sci. 31 (2007) 85–94, https://doi.org/10.1016/j.ejps.2007.02.009.
[63] S. Bogusz, R.M. Venable, R.W. Pastor, Molecular Dynamics Simulations of Octyl Glucoside Micelles : Structural Properties, (2000), pp. 5462–5470.
[64] D.P. Tieleman, D. van der Spoel, H.J.C. Berendsen, Molecular dynamics simulations of dodecylphosphocholine micelles at three different aggregate sizes: micellar structure and chain relaxation, J. Phys. Chem. B 104 (2000) 6380–6388, https://doi.org/10.1021/jp001268f.
[65] J. Ulmius, G. Lindblom, H. Wennerström, L.B.Å. Johansson, K. Fontell, O. Söderman, G. Arvidson, Molecular organization in the liquid-crystalline phases of lecithin-sodium cholate-water systems studied by nuclear magnetic resonance, Biochemistry. 21 (1982) 1553–1560, https://doi.org/10.1021/bi00536a014.
[66] D.A. Fahey, M.C. Carey, J.M. Donovan, Bile acid/phosphatidylcholine interactions in mixed monomolecular layers: differences in condensation effects but not interfacial orientation between hydrophobic and hydrophilic bile acid species, Biochemistry. 34 (1995) 10886–10897, https://doi.org/10.1021/bi00034a023.
[67] P.B. Welzel, H.K. Cammenga, Equilibrium penetration of DMPC monolayers by sodium cholate, J. Colloid Interface Sci. 207 (1998) 70–77, https://doi.org/10.1006/jcis.1998.5765.
[68] A. Tiss, S. Ransac, H. Lengsfeld, P. Hadvàry, A. Cagna, R. Verger, Surface behaviour of bile salts and tetrahydrolipstatin at air/water and oil/water interfaces, Chem. Phys. Lipids 111 (2001) 73–85, https://doi.org/10.1016/S0009-3084(01)00149-9.
[69] M. Vadnere, S. Lindenbaum, Distribution of bile salts between 1-octanol and aqueous buffer, J. Pharm. Sci. 71 (1982) 875–881, https://doi.org/10.1002/jps.2600710809.
[70] S.R. Euston, U. Bellstedt, K. Schillbach, P.S. Hughes, The adsorption and competitive adsorption of bile salts and whey protein at the oil-water interface, Soft Matter 7 (2011) 8942–8951, https://doi.org/10.1039/c1sm05840a.
[71] D.M. Small, Physicochemical studies of cholesterol gallstone formation, Gastroenterology. 52 (1967) 607–610, https://doi.org/10.1016/S0016-5085(67)80190-2.
[72] W. Shankland, The equilibrium and structure of lecithin-cholate mixed micelles, Chem. Phys. Lipids 4 (1970) 109–130, https://doi.org/10.1016/0009-3084(70)90042-3.
[73] N.A. Mazer, M.C. Carey, G.B. Benedek, Micellization, Solubilization, and Microemulsions, Plenum Press, New York, 1977.
[74] N.A. Mazer, G.B. Benedek, M.C. Carey, Size and shape of bile-salt (bs), bs-lecithin (l) and bs-l-cholesterol (ch) micelles using quasi-elastic light-scattering spectroscopy, Gastroenterology. 70 (1976) 998.
[75] J. Leng, S.U. Egelhaaf, M.E. Cates, Kinetics of the micelle-to-vesicle transition: aqueous lecithin-bile salt mixtures, Biophys. J. 85 (2003) 1624–1646, https://doi.org/10.1016/S0006-3495(03)74593-7.
[76] B. Ashok, S. Ayd, K. Son, H. Önyüksel, Bile salt-phospholipid mixed micelles as solubilizers for water-insoluble drugs, FABAD, J. Pharm. Sci. 28 (2003) 161–172.
[77] W. Shankland, Structural phase relationships in lecithin-cholate- water systems, Chem. Phys. Lipids 19 (1977) 20–42.
[78] J.S. Pedersen, S.U. Egelhaaf, P. Schurtenberger, Formation of Polymerlike mixed micelles and vesicles in lecithin—bile salt solutions: a Small-angle neutron-scattering study, J. Phys. Chem. 99 (1995) 1299–1305, https://doi.org/10.1021/j100004a033.
[79] R.P. Hjelm, C. Schteingart, A.F. Hoffmann, D.S. Sivia, Form and structure of self-assembling particles in monoolein-bile salt mixtures, J. Phys. Chem. 99 (1995) 16395–16406, https://doi.org/10.1021/j100044a030.
[80] R.E. Stark, G.J. Gosselin, J.M. Donovan, M.C. Carey, M.F. Roberts, Influence of dilution on the physical state of model bile systems: NMR and quasi-elastic light-scattering investigations, Biochemistry. 24 (1985) 5599–5605, https://doi.org/10.1021/bi00341a047.
[81] M.a. Kiselev, M. Janich, a. Hildebrand, P. Strunz, R.H.H. Neubert, D. Lombardo, Structural transition in aqueous lipid/bile salt [DPPC/NaDC] supramolecular aggregates: SANS and DLS study, Chem. Phys. 424 (2013) 93–99, https://doi.org/10.1016/j.chemphys.2013.05.014.
[82] R.L. Thurmond, G. Lindblom, M.F. Brown, Effect of bile salts on monolayer curvature of a phosphatidylethanolamine/water model membrane system, Biophys. J. 60 (1991) 728–732.
[83] A. Walter, P.K. Vinson, A. Kaplun, Y. Talmon, Intermediate structures in the cholate-phosphatidylcholine vesicle micelle transition, Biophys. J. 60 (1991) 1315–1325.